Mechanism of the formation of proton transfer pathways in photosynthetic reaction centers

Yu Sugo[a], Keisuke Saito[a,b], and Hiroshi Ishikita[a,b,1]

[a]Department of Applied Chemistry, University of Tokyo, Tokyo 113-8654, Japan; and [b]Research Center for Advanced Science and Technology, University of Tokyo, Tokyo 153-8904, Japan

Edited by Arieh Warshel, University of Southern California, Los Angeles, CA, and approved June 16, 2021 (received for review February 17, 2021)

In photosynthetic reaction centers from purple bacteria (PbRCs) from *Rhodobacter sphaeroides*, the secondary quinone Q_B accepts two electrons and two protons via electron-coupled proton transfer (PT). Here, we identify PT pathways that proceed toward the Q_B binding site, using a quantum mechanical/molecular mechanical approach. As the first electron is transferred to Q_B, the formation of the Grotthuss-like pre-PT H-bond network is observed along Asp-L213, Ser-L223, and the distal Q_B carbonyl O site. As the second electron is transferred, the formation of a low-barrier H-bond is observed between His-L190 at Fe and the proximal Q_B carbonyl O site, which facilitates the second PT. As Q_BH_2 leaves PbRC, a chain of water molecules connects protonated Glu-L212 and deprotonated His-L190 forms, which serves as a pathway for the His-L190 reprotonation. The findings of the second pathway, which does not involve Glu-L212, and the third pathway, which proceeds from Glu-L212 to His-L190, provide a mechanism for PT commonly used among PbRCs.

proton-coupled electron transfer | low-barrier hydrogen bond | photosystem II | conformational gating | artificial photosynthesis

Purple bacterial photosynthetic reaction centers (PbRCs) have special pair bacteriochlorophylls (P_L/P_M), accessory bacteriochlorophylls (B_L/B_M), bacteriopheophytins (H_L/H_M), and ubiquinones (Q_A/Q_B) in the heterodimeric L/M protein subunit pair. P_L and P_M form the electronically coupled special pair [P_LP_M]. The electronic excitation of [P_LP_M] leads to the formation of the charge-separated state, $[P_LP_M]^{\bullet+}B_L^{\bullet-}$, and subsequent electron transfer occurs to Q_B via H_L and Q_A (1–3). Q_B accepts two electrons via Q_A and two protons via the proton transfer (PT) pathways, forming Q_BH_2, and leaves the PbRC.

The first and second electron transfers from Q_A to Q_B occur with rates $k_{AB}^{(1)}$ (10^4 s^{-1}) and $k_{AB}^{(2)}$ (10^3 s^{-1}), respectively (4). The first PT leads to the protonation of the distal and carbonyl O site of Q_B (with respect to the nonheme Fe). The proton donor of the distal Q_B O site is Ser-L223, for which the H-bond donor is Asp-L213. The Ser-L223 side chain, which donates an H-bond with Asp-L213 due to the highly polarized carboxyl O site, reorients toward the distal Q_B O site in response to $Q_B^{\bullet-}$ formation (5, 6). Notably, in photosystem II (PSII), D1-Ser264 and D1-His252, which correspond to Ser-L223 and Asp-L213 in the PbRC, respectively (7), serve as a PT pathway toward the distal Q_B O site (8). As D(L213)N (9) and S(L223)A (10, 11) mutations decrease the $k_{AB}^{(2)}$ significantly, these residues are likely involved in the PT pathway toward the distal Q_B O site in the PbRC. Although Asp-H124, His-H126, and His-H128 are likely to form the entry point of the major PT pathway (12), it also seems plausible that the PT pathway is delocalized toward the protein bulk surface (13–15). The delocalization of the PT pathway is also observed in PSII; specifically, the PT pathway is branched as it proceeds from the oxygen-evolving complex via D1-Asp61 toward the protein bulk surface (16).

Glu-L212 is the titratable residue that is nearest to and a candidate for the proton donor to the proximal Q_B O site. Indeed, the uptake of 0.3 to 0.8 H^+ by Glu-L212 has been reported upon $Q_B^{\bullet-}$ formation (17–21). The protonation of Glu-L212 plays a role in electron transfer, increasing the redox potential $E_m(Q_B)$ with respect to $E_m(Q_A)$ (22). However, the PT pathway from Glu-L212 to Q_BH^- is unclear (4), because the crystal structure shows that Glu-L212 cannot form an H-bond with the proximal Q_B O site (Glu-L212...Q_B = 5.7 Å) (23). PT occurs most efficiently along H-bonds (24). Okamura et al. (4) proposed that the movement of Q_BH^- toward Glu-L212 and the formation of an H-bond might be required for PT. Alternatively, His-L190, which forms an H-bond with the proximal Q_B O site (His-L190...Q_B = 2.81 Å) (23), might serve as a proton donor for Q_BH^-, as proposed by Wraight (25). However, Wraight also argued that the pK_a value for the deprotonation of singly protonated His-L190 might be too high even in the presence of the cationic nonheme Fe.

Notably, the crystal structures of PSII and PbRC show large structural similarity (7). His-L190 is conserved as D1-His215 at the nonheme Fe complex in PSII (7). In PSII, D1-His215 can form a low-barrier H-bond with Q_BH^-, which facilitates Q_BH_2 formation (8, 26, 27). Low-barrier H-bonds can form when the pK_a values of the H-bond donor and acceptor moieties are nearly equal (28, 29). The shape of the potential energy curve of a low-barrier H-bond is symmetric, while that of a standard H-bond is asymmetric because pK_a(donor) > pK_a(acceptor) (30) (Fig. 1). In addition, Glu-L212 in PbRCs is not conserved as a titratable residue in PSII. These findings for PSII might provide an opportunity to revisit the mechanism of PT toward the proximal Q_B O site in PbRCs. Here, we report how PT pathways form in response to electron transfer in the PbRC protein environment, by adopting a large-scale quantum mechanical/molecular mechanical (QM/MM) approach based on the PbRC crystal structure (23).

Significance

The crystal structures of photosynthetic reaction centers from purple bacteria (PbRCs) and photosystem II show large structural similarity. However, the proposed mechanisms of proton transfer toward the terminal electron acceptor quinone (Q_B) are not consistent. In particular, not His-L190, which is an H-bond partner of Q_B, but rather Glu-L212, which is ∼6 Å away from Q_B, was assumed to be the direct proton donor for Q_B. We demonstrate that the H-bond between His-L190 and Q_B is a low-barrier H-bond, which facilitates proton transfer from singly protonated His-L190 to Q_B. Furthermore, Glu-L212 is not a direct H-bond donor for Q_B. However, it facilitates proton transfer toward deprotonated His-L190 via water molecules after Q_BH_2 forms and leaves the PbRC.

Author contributions: H.I. designed research; Y.S., K.S., and H.I. performed research; Y.S., K.S., and H.I. analyzed data; and H.I. wrote the paper.

The authors declare no competing interest.

This article is a PNAS Direct Submission.

[1]To whom correspondence may be addressed. Email: hiro@appchem.t.u-tokyo.ac.jp.

This article contains supporting information online at https://www.pnas.org/lookup/suppl/doi:10.1073/pnas.2103203118/-/DCSupplemental.

Published July 23, 2021.

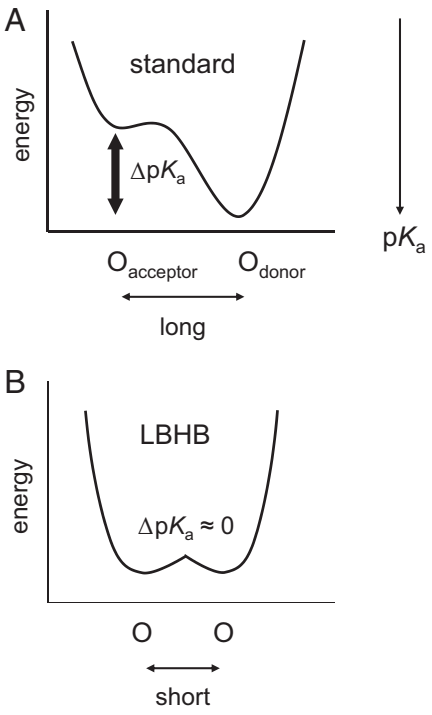

Fig. 1. Typical potential-energy profiles of H-bonds. (*A*) Standard H-bond. (*B*) Low-barrier H-bond (LBHB). In low-barrier H-bonds, the H-bond acceptor ($O_{acceptor}$) and donor (O_{donor}) cannot be distinguishable due to the same pK_a values.

Results

The PbRC crystal structure shows that the H-bond network proceeds from the distal Q_B carbonyl O site via Ser-L223, Asp-L213, a water molecule, and Asp-M17 (23) (i.e., QM region) (Fig. 2). Note that Asp-L210 cannot form an H-bond with the residues in the H-bond network, since it is more than 5.0 Å away from the nearest residue, Asp-M17 (23). When the first electron transfer occurs to Q_B, Glu-L212 protonates and the Ser-L223 hydroxyl group, which initially forms an H-bond with Asp-L213, reorients toward $Q_B^{\bullet-}$ (6, 31, 32). The H-bond distances along the Q_B...Ser-L223...Asp-L213...H_2O...Asp-M17 decrease in response to the proton uptake of Glu-L212 and the reorientation of the Ser-L223 hydroxyl group (Table 1). Specifically, the H-bond between the distal Q_B O site and Ser-L223 is shortened from 2.65 to 2.55 Å in response to $Q_B^{\bullet-}$ formation (Table 1), which implies that the first PT proceeds toward the distal Q_B O site. The potential energy profile indicates that PT is energetically downhill from Ser-L223 to the distal Q_B O site in the presence of $Q_B^{\bullet-}$ (Fig. 3*A*).

Asp-M17 has been reported to be involved in the PT pathway (33). When it accepts a proton from the bulk region, the entire H-bond network that proceeds from Asp-M17 via a water molecule, Asp-L213, and Ser-L223 forms the pre-PT H-bond pattern (Fig. 2*B*), which serves as a downhill pathway (Fig. 3*A*): the proton at Asp-M17 is ultimately transferred to the distal Q_B O site concertedly via the Grotthuss-like mechanism.

The water molecule that connects Asp-M17 and Asp-L213 (W-H267) is present in the 2.01-Å crystal structure reported by Fujii and colleagues (34) (PDB ID code 3I4D), whereas it is absent in the light-exposed $Q_B^{\bullet-}$ structure reported by Stowell et al. (23) at 2.60-Å resolution (PDB ID code 1AIG). It should also be noted that the distribution pattern of water molecules shows that the Asp-L213 and Asp-M17 moieties are highly accessible from the protein bulk surface (Fig. 4*A*). Thus, Asp-L213...Ser-L223...Q_B is likely to be the essential component for the first PT, as the corresponding H-bond network, D1-His252...D1-Ser264...Q_B is conserved in PSII (8). Consistently, the potential energy profile indicates that the proton at Asp-L213 can be transferred via Ser-L223 to the distal Q_B O site along a downhill pathway even if Asp-M17 is ionized (Fig. 3*B*).

As the Q_BH^- forms (via the first PT and the second electron transfer), the H-bond between His-L190 and the proximal Q_B O site is significantly shortened to 2.49 Å (Table 1). The potential-energy profile for the H-bond between His-L190 and the proximal Q_B O site resembles that for a typical low-barrier H-bond (Fig. 3*C*), as observed for the H-bond between D1-His215 and the proximal Q_B O site in PSII (8, 26, 27). Thus, the second PT can proceed along the barrierless potential, leading to the release of Q_BH_2 from the PbRC.

Not only the crystal structure (23) but also the calculated distribution pattern of water molecules shows that no H-bond network exists between Glu-L212 and His-L190 in the presence of Q_B (Fig. 4*A*). In contrast, the Q_B-lacking crystal structure shows that water molecules form an H-bond network that connects Glu-L212 and His-L190 (e.g., PDB ID code 1L9B) (35) (Fig. 4*B*), which may also be the case with the Q_BH_2-released PbRC. QM/MM calculations also indicate that an H-bond network forms among protonated Glu-L212, water molecules, and deprotonated His-L190 (Fig. 5*A*). The potential-energy profile along the H-bond network suggests that pK_a(Glu-L212) ~ pK_a(His-L190) (Fig. 5*B*).

The distribution pattern of water molecules suggests that there are more water molecules than are identified at the Q_B binding moiety in the crystal structure (Fig. 4*B*). As the addition of a water molecule to the H-bond network (Fig. 5*C*) decreases the energy barrier for the PT (Fig. 5*D*), the existence of water molecules, which are not visible in the reported crystal structure, may facilitate PT from Glu-L212 to His-L190 in the Q_BH_2-released PbRC.

Discussion

The initial protonation of Q_B occurs at the distal O site, as the H-bond between Ser-L223 and the distal Q_B O site is specifically shortened in response to the formation of $Q_B^{\bullet-}$ (Fig. 2*A* and *B*). The present results indicate that Ser-L223, Asp-L213, a water molecule, and Asp-M17 form a Grotthuss-like PT pathway toward the distal Q_B O site (Figs. 2*B* and 3*A*). Among them, protonated Asp-L213 (5, 22, 31, 36–38) [pK_a(Asp-L213) = 8.9 (38)] and Ser-L223 are conserved as D1-His252 and D1-Ser264 in PSII, respectively (39). Because D1-His252 and D1-Ser264 serve as a PT pathway toward the distal Q_B O site in PSII (8), Ser-L223 and Asp-L213 are the primary components for PT toward the distal Q_B O site in the PbRC. Consistently, the D(L213)N (9) and S(L223)A (10, 11) mutations affected $k_{AB}^{(2)}$ by factors of 6,000 and 400, respectively, whereas the D(M17)N mutation affected $k_{AB}^{(2)}$ only by a factor of 2 (4). The extension of the H-bond network [e.g., Asp-M17, Asp-L210 (33, 40), Asp-H124, His-H126, His-H128 (12, 41), and water molecules] may increase the surface of the proton entry point. It seems plausible that the proton can enter either directly from Asp-L213 or the extension of the H-bond network.

Glu-L212 was assumed to serve as a proton donor to the proximal Q_B O site (e.g., refs. 4, 42, and 43). However, Glu-L212 cannot form an H-bond with Q_B and is unlikely to serve as a direct proton donor for Q_B, because PT occurs most efficiently along H-bonds (24). The findings of His-L190 forming a low-barrier H-bond with the proximal Q_B O site and being able to serve as a direct proton donor to Q_BH^- (Fig. 3*C*) suggest that pK_a(His-L190) ~ pK_a(Q_BH^-/Q_BH_2). The involvement of His-L190 in Q_BH_2 formation is consistent with the mechanism proposed by Wraight (25) and the mechanism suggested for PSII (8, 26, 27). In PSII, QM/MM calculations showed that D1-His215 forms a low barrier H-bond with Q_BH^-, facilitating PT (8, 26).

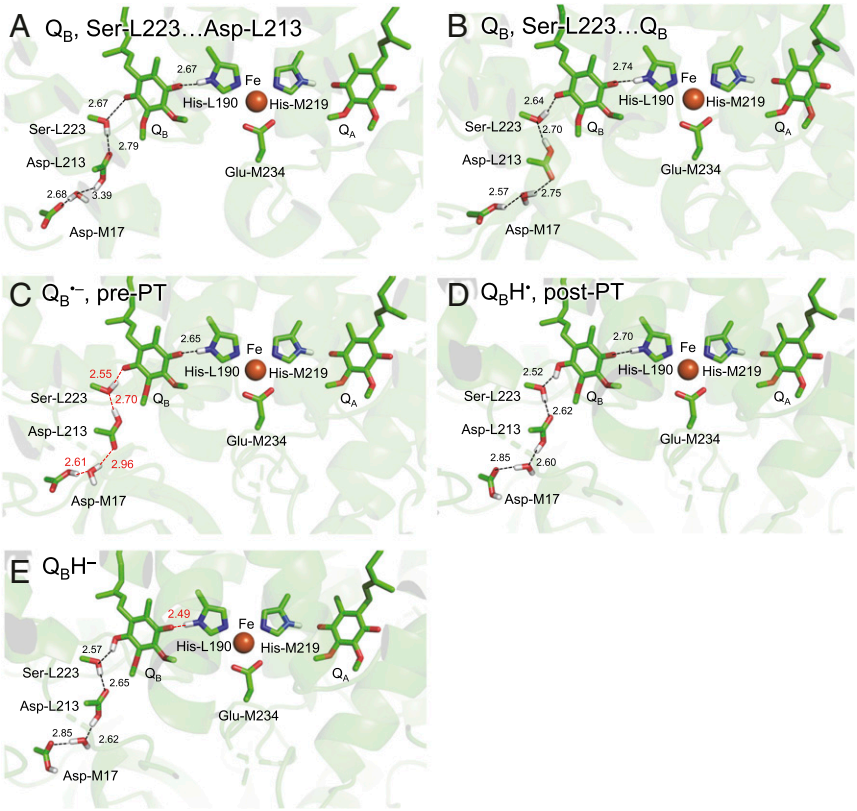

Fig. 2. H-bond network of Q_B. (*A*) Q_B (before the first electron transfer): Ser-L223 donates an H-bond to Asp-L213. (*B*) Q_B: Ser-L223 donates an H-bond to Q_B. (*C*) $Q_B^{\bullet-}$ (after the first electron transfer) in the pre-PT H-bond pattern. (*D*) $Q_BH^{\bullet}$ in the post-PT H-bond pattern. (*E*) Q_BH^- (after the second electron transfer). Black dotted lines indicate H-bonds. Red dotted lines indicate proton-conducting H-bonds. H atoms in the H-bond network are depicted as white sticks. Note that Glu-L212 is deprotonated in neutral unprotonated Q_B and protonated in other states.

Recent Fourier transform infrared (FTIR) studies suggested that D1-His215 can serve as a proton donor to anionic Q_BH^-, as D1-His215 releases the proton upon the oxidation of the nonheme Fe complex (27). His-L190 is conserved as D1-His215 at the nonheme Fe cluster in PSII, whereas Glu-L212 is not conserved. These features suggest that His-L190 is the proton donor for the proximal O site of Q_B in the PbRC.

The Q_B binding pocket has a large cavity. The Q_BH_2 channel is oriented toward the protein bulk surface in the transmembrane region (44) (Fig. 4*B*). Although the energy barrier for PT

Table 1. H-bond distances near Q_B (Å)

	PT pattern	L190…Q_B	Q_B…L223	L223…L213	L213…H_2O	H_2O…M17
PDB						
1AIG*		2.81	3.21	3.07	—	—
3I4D†		2.57	2.60	2.51	2.73	3.53
QM/MM						
[deprotonated Glu-L212]‡						
Q_B	L223…L213§	2.67	2.67	2.79	3.39	2.68
Q_B	L223…Q_B¶	2.74	2.64	2.70	2.75	2.57
[protonated Glu-L212]‡						
$Q_B^{\bullet-}$	pre-PT#	2.65	**2.55**	2.70	2.98	2.61
$Q_BH^{\bullet}$	post-PT#	2.70	**2.52**	2.62	2.60	2.85
Q_BH^-	pre-PT#	**2.49**	2.57	2.65	2.62	2.85
Q_BH_2	post-PT	2.60	2.57	2.64	2.62	2.86

—, not applicable. Distances of low-barrier H-bonds are in bold.
*Reported as the light-exposed charge-separated $Q_B^{\bullet-}$ structure (23). The distances in the dark-adapted structure (PDB ID code 1AIJ) (23) are not shown: the Q_B binding site in the dark-adapted structure is not consistent with that in the light-exposed structure (23), whereas the difference in the Q_B binding site is not observed in a FTIR difference spectroscopy (67).
†The redox state is not reported (34).
‡Glu-L212 is deprotonated for neutral unprotonated Q_B and protonated for $Q_B^{\bullet-}$ in the present calculation.
§Ser-L223 donates an H-bond to Asp-L213 (Fig. 2*A*).
¶Ser-L223 donates an H-bond to Q_B (Fig. 2*B*).
#See Fig. 2.

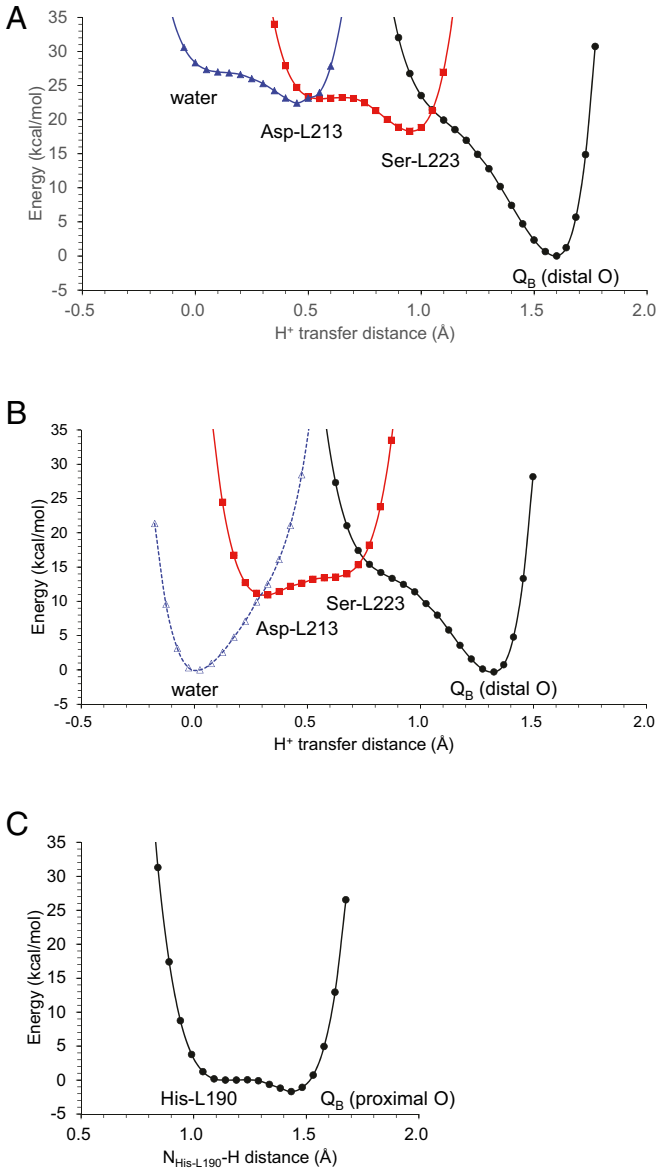

Fig. 3. Potential-energy profiles for the first and second PT processes. (*A*) PT toward the distal Q_B O site in the presence of (*A*) protonated Asp-M17 and (*B*) ionized Asp-M17. The potential-energy profile was calculated, modeling a water molecule at the Asp-M17 and Asp-L213 moieties, which is observed in the crystal structure reported by Fujii and colleagues (34) (PDB ID code 3I4D). (*C*) PT toward the proximal Q_B O site.

from Glu-L212 to His-L190 is not significantly low with respect to PT to the distal (Fig. 3 *A* and *B*) and proximal Q_B O (Fig. 3*C*) sites, the PT profile suggests that pK_a(His-L190) ~ pK_a(Glu-L212) (= 9.4) (38) (Fig. 5 *B* and *D*), which would make the protonation of His-L190 by Glu-L212 possible before an unprotonated quinone occupies the Q_B binding site. The H-bond network presented here is likely to represent a minimum component of the reprotonation pathway for ionized His-L190, which is consistent with the mechanism proposed by Wraight (25), specifically a water molecule serving as a direct proton donor to reprotonate ionized His-L190. Cherepanov et al. (45) proposed that the H-bond network that connects Glu-L212 and His-L190 (water bridge) forms in response to the release of Q_BH_2 and prevents the Q_BH_2 to Q_BH^- reversion. The estimated Q_B exchange time is ~1 ms (46), which is sufficiently long for a few water molecules to approach the Q_B binding site and form the H-bond network: for example, among 103 water molecules in the protein interior near the Mn_4CaO_5 cluster of the PSII crystal structure, 90 water molecules are incorporated into the binding positions in the 50-ns molecular dynamics simulation (47). In addition, some PbRC crystal structures show that the corresponding water molecule also exists near Glu-L212 and His-L190 even when Q_B is only slightly displaced from His-L190 in the binding pocket (e.g., PDB ID code 1AIJ) (23).

The PbRC crystal structure shows that Glu-L212 has an H-bond network that proceeds toward the protein bulk surface [e.g., the P1a and P1b water chains (48)], which may serve as a pathway for the uptake of 0.3 to 0.8 H^+ (17, 18) for ionized Glu-L212

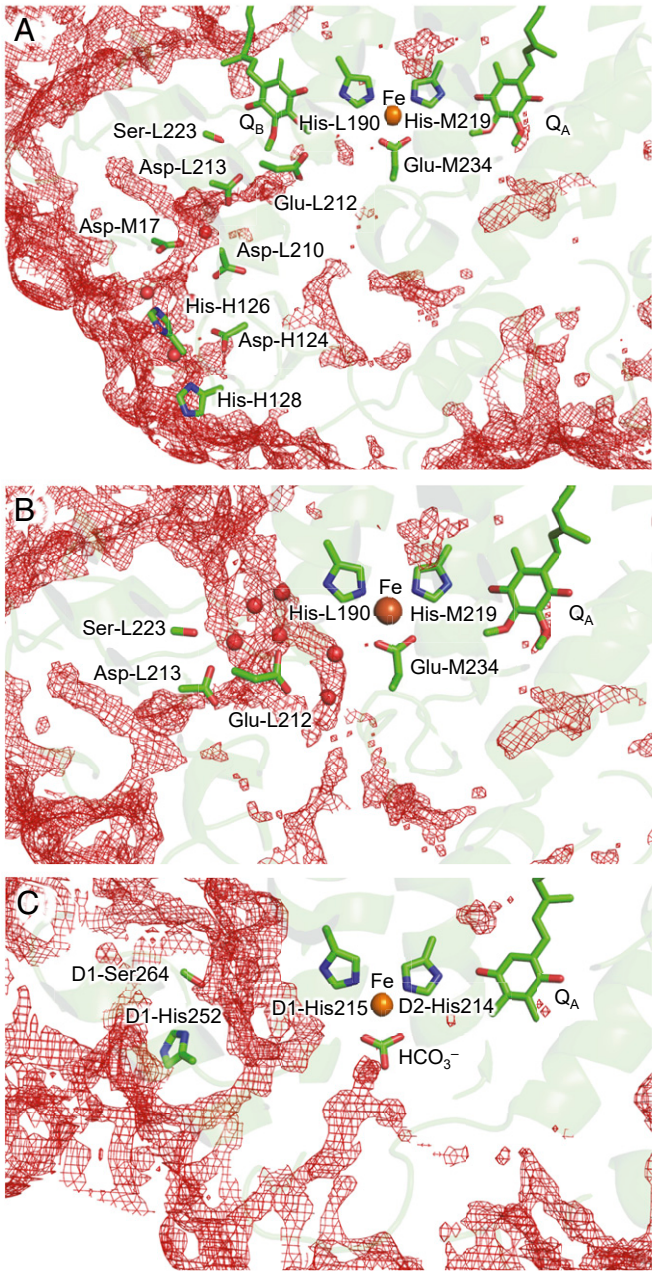

Fig. 4. Distribution patterns of water molecules (red mesh). (*A*) In the presence of Q_B in PbRC (PDB ID code 1AIG) (23). (*B*) In the absence of Q_B in the PbRC. Q_B was removed from the PbRC crystal structure. (*C*) In the absence of Q_B in PSII (PDB ID code 3JCU) (66). The threshold of 3D distribution function is 2.0.

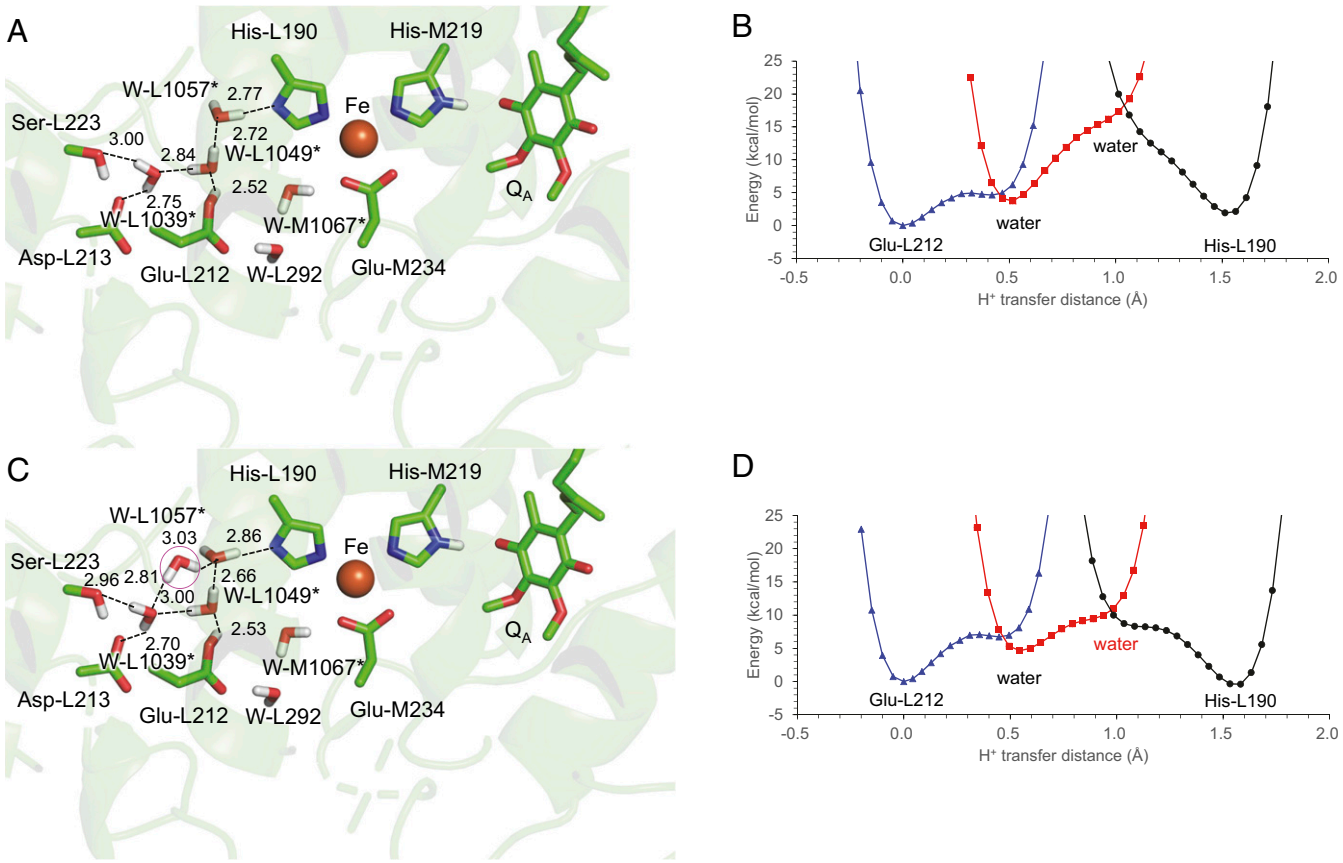

Fig. 5. (*A*) H-bond network that connects protonated Glu-L212 and ionized His-L190 in the absence of Q_B and (*B*) the potential-energy profile. The potential-energy profile was calculated adding four water molecules (*: L1039, L1049, L1057, and M1067), which are visible in the Q_B-lacking crystal structure (PDB ID code 1L9B) (35). (*C*) Addition of a water molecule (pink circle) to the H-bond network and (*D*) the potential-energy profile.

(19–21) upon $Q_B^{\bullet-}$ formation (Fig. 6, panel 1). The protonation of Glu-L212 increases $E_m(Q_B)$ with respect to $E_m(Q_A)$, leading to an energetically downhill electron transfer to Q_B (22). As $Q_B^{\bullet-}$ forms, the -OH group of Ser-L223 is oriented away from Asp-L213 toward the distal Q_B O site, further increasing $E_m(Q_B)$ (6), transforming the post-PT (Fig. 6, panel 4) into pre-PT patterns (Fig. 6, panel 1), and facilitating $Q_BH^{\bullet}$ formation (6) (Fig. 6, panel 2). Thus, Glu-L212 plays a role in facilitating the first electron transfer to Q_B, donating a proton to ionized His-L190 in the absence of Q_B (Fig. 6, panel 4), and eventually providing the second proton for transfer to Q_BH^- via His-L190 (Fig. 6, panel 3).

Remarkably, Glu-L212 is not conserved in PSII. The absence of a subunit H-like protein in PSII renders D1-His215 (i.e., Asp-L213 in PbRC) exposed to the protein bulk surface (Fig. 4*C*), which may explain why PSII has no corresponding protonatable residue. Because subunit H is likely to restrict the access of water molecules to the Q_B binding pocket in the PbRC, having protonated Glu-L212 in the Q_B binding pocket could be advantageous for the immediate reprotonation of ionized His-L190 and binding of unprotonated Q_B at protonated His-L190.

In summary, the pathway to the distal Q_B O site is a Grotthuss-like H-bond network (e.g., Ser-L223 and Asp-L213), which facilitates PT by transforming the pre-PT to post-PT H-bond patterns (Fig. 2 *B* and *C*). In contrast, the pathway to the proximal Q_B O site is a single, low-barrier H-bond between Q_BH^- and His-L190 (Fig. 2*D*), as observed in PSII (8, 26, 27). His-L190 is the proton donor for Q_BH^- and no movement of Q_BH^- toward Glu-L212 (e.g., ref. 4) is required for the Q_BH^- protonation. However, Glu-L212 is ultimately involved in PT to Q_BH^-, because protonated Glu-L212 is likely to serve as a proton donor to ionized His-L190 via water molecules in response to the release of Q_BH_2 (Fig. 5). Moreover, the proton delivered to Glu-L212 during the initial photo-cycle is delivered to Q_BH^- during the next photo-cycle (Fig. 6). The mechanism presented here can also explain why Glu-L212 is crucial for PT (e.g., refs. 5 and 17–22) irrespective of the absence of an H-bond with Q_B (see discussions in ref. 4) and how the protonation of Q_BH^- to Q_BH_2 proceeds via His-L190 (25).

Methods

Coordinates and Atomic Partial Charges. The atomic coordinates were taken from the X-ray structure of PbRC from *Rhodobacter sphaeroides* (PDB ID code 1AIG) (23). The H atom positions were optimized with CHARMM (49), whereas the heavy atom positions were fixed. During the procedure, all titratable groups (e.g., acidic and basic groups) were ionized. Atomic partial charges of the amino acids were obtained from the CHARMM22 (50) parameter set, whereas those of cofactors were obtained from the previous studies (51). Additional counter ions were added to neutralize the entire system in QM/MM calculations.

Protonation Pattern. The computation was based on the electrostatic continuum model, solving the linear Poisson–Boltzmann equation with the MEAD program (52). The difference in electrostatic energy between the two protonation states, protonated and deprotonated, in a reference model system was calculated using a known experimentally measured pK_a value [e.g., 4.0 for Asp (53)]. The difference in the pK_a value of the protein relative to the reference system was added to the known reference pK_a value. The experimentally measured pK_a values employed as references were 12.0 for Arg, 4.0 for Asp, 9.5 for Cys, 4.4 for Glu, 10.4 for Lys, 9.6 for Tyr (53), and 7.0 and 6.6 for the N_ε and N_δ atoms of His, respectively (54–56). All other titratable sites were fully equilibrated to the protonation state of the target site during titration. The dielectric constants were set to 4 inside the protein

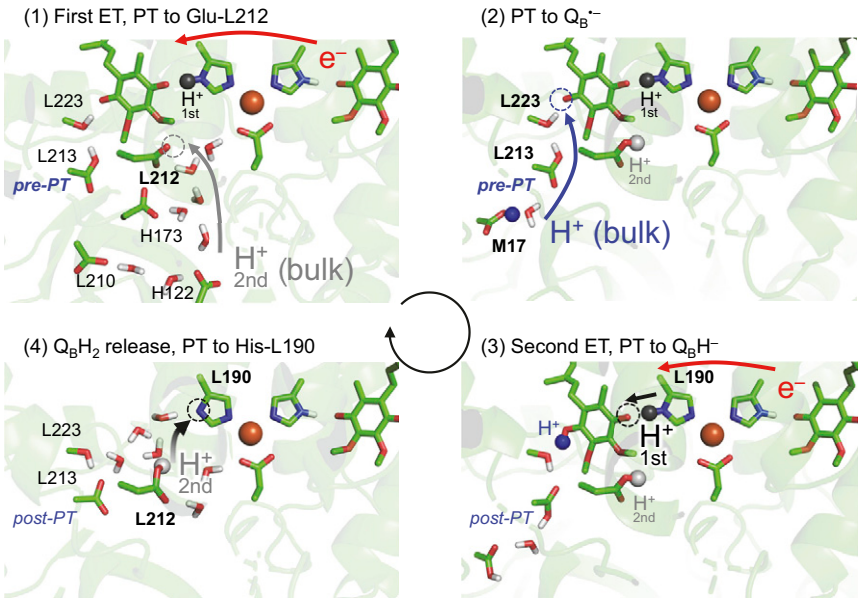

Fig. 6. Overview of PT (blue and gray arrows) and electron transfer (ET, red arrows). PT events toward the distal/proximal Q_B O site are gray/blue colored, respectively. Proton acceptor sites are indicated by dotted circles. H^+-first already exists at His-L190 (panel 1) and is transferred to the proximal Q_B O site (panel 3). H^+-second is transferred from the bulk water region to deprotonated Glu-L212 (panels 1 to 2) and is further transferred to deprotonated His-L190 (panel 4), being H^+-first in the next turnover.

and 80 for water. All computations were performed at 300 K, pH 7.0, and with an ionic strength of 100 mM. The linear Poisson–Boltzmann equation was solved using a three-step grid-focusing procedure at resolutions of 2.5, 1.0, and 0.3 Å. The ensemble of the protonation patterns was sampled by the Monte Carlo method with the Karlsberg program (57). The Monte Carlo sampling yielded the probabilities [protonated] and [deprotonated] of the two protonation states of the molecule.

QM/MM Calculations. The unrestricted density functional theory method was employed with the B3LYP functional and LACVP* basis sets, using the QSite (58) program. In the QM region, all the atomic coordinates were fully relaxed. In the MM region, the positions of H atoms were optimized using the OPLS2005 force field, while the positions of heavy atoms were fixed. The initial-guess wavefunctions were obtained using the ligand field theory (59) implemented in the QSite program. To analyze the potential-energy profiles for PT to Q_B, the QM region was defined as Q_B, the nonheme Fe complex (Fe, the side-chains of His-L190, His-L230, His-M219, His-M266, and Glu-M234), the side-chains of Asp-M17, Asp-L213, and Ser-L223, and a water molecule at the Asp-M17 and Asp-L213 moiety, which is visible in the 2.01-Å crystal structure (34) (PDB ID code 3I4D). To analyze the potential-energy profiles for PT from protonated Glu-L212 to ionzed His-L190 in the absence of Q_B, Q_B was removed and the QM region was defined as the nonheme Fe complex (Fe, the side-chains of His-L190, His-L230, His-M219, His-M266, and Glu-M234), the side-chains of Glu-L212, Asp-L213, and Ser-L223, and five water molecules (W-L292, L1039, L1049, L1057, and M1067), which are visible in the Q_B-lacking crystal structure (PDB ID code 1L9B) (35) if not otherwise specified. All other protein units and cofactors were approximated by the MM force field (i.e., electrostatic influences are sufficiently considered in the MM region). Note that the residues in the PT pathways must be included in the QM region to consider the formation/breakage of the covalent (H-) bonds during PT. See Dataset S1 for the atomic coordinates of the resulting QM region.

The potential-energy profiles of H-bonds were obtained as follows. First, we prepared the QM/MM optimized geometry without constraints and used the resulting geometry as the initial geometry. The H atom under investigation was then moved from the H-bond donor atom (O/N_{donor}) toward the acceptor atom ($O/N_{acceptor}$) by 0.05 Å, after which the geometry was optimized by constraining the O/N_{donor}–H and H–$O/N_{acceptor}$ distances. The energy of the resulting geometry was calculated. This procedure was repeated until the H atom reached the $O/N_{acceptor}$ atom.

Analysis of Water Molecule Distribution in the Protein. To analyze the distribution of water molecules in the protein environment, we used a three-dimensional reference interaction site model (3D-RISM) with Placevent analysis (60–64). It should be noted that the distribution pattern of water molecules obtained from the 3D-RISM with Placevent analysis was consistent with the positions of the water molecules (65).

Data Availability. All study data are included in the article and Dataset S1.

ACKNOWLEDGMENTS. This research was supported by Japan Science and Technology Core Research for Evolutionary Science and Technology (JST CREST) Grant JPMJCR1656 (to H.I.); Japan Society for the Promotion of Science (JSPS) Grants KAKENHI JP18H01937, JP18H05155, JP20H03217, and JP20H05090 (to H.I.) and JP16H06560 and JP18H01186 (to K.S.); and the Interdisciplinary Computational Science Program in Computational Sciences, University of Tsukuba.

1. K. L. Zankel, D. W. Reed, R. K. Clayton, Fluorescence and photochemical quenching in photosynthetic reaction centers. *Proc. Natl. Acad. Sci. U.S.A.* **61**, 1243–1249 (1968).
2. U. Finkele, C. Lauterwasser, W. Zinth, K. A. Gray, D. Oesterhelt, Role of tyrosine M210 in the initial charge separation of reaction centers of *Rhodobacter sphaeroides*. *Biochemistry* **29**, 8517–8521 (1990).
3. H. Tamura, K. Saito, H. Ishikita, Acquirement of water-splitting ability and alteration of the charge-separation mechanism in photosynthetic reaction centers. *Proc. Natl. Acad. Sci. U.S.A.* **117**, 16373–16382 (2020).
4. M. Y. Okamura, M. L. Paddock, M. S. Graige, G. Feher, Proton and electron transfer in bacterial reaction centers. *Biochim. Biophys. Acta* **1458**, 148–163 (2000).
5. E. G. Alexov, M. R. Gunner, Calculated protein and proton motions coupled to electron transfer: Electron transfer from Q_A^- to Q_B in bacterial photosynthetic reaction centers. *Biochemistry* **38**, 8253–8270 (1999).
6. H. Ishikita, E.-W. Knapp, Variation of Ser-L223 hydrogen bonding with the Q_B redox state in reaction centers from *Rhodobacter sphaeroides*. *J. Am. Chem. Soc.* **126**, 8059–8064 (2004).
7. H. Michel, J. Deisenhofer, Relevance of the photosynthetic reaction center from purple bacteria to the structure of photosystem II. *Biochemistry* **27**, 1–7 (1988).
8. K. Saito, A. W. Rutherford, H. Ishikita, Mechanism of proton-coupled quinone reduction in Photosystem II. *Proc. Natl. Acad. Sci. U.S.A.* **110**, 954–959 (2013).
9. E. Takahashi, C. A. Wraight, A crucial role for AspL213 in the proton transfer pathway to the secondary quinone of reaction centers from *Rhodobacter sphaeroides*. *Biochim. Biophys. Acta* **1020**, 107–111 (1990).
10. M. L. Paddock, P. H. McPherson, G. Feher, M. Y. Okamura, Pathway of proton transfer in bacterial reaction centers: Replacement of serine-L223 by alanine inhibits electron and proton transfers associated with reduction of quinone to dihydroquinone. *Proc. Natl. Acad. Sci. U.S.A.* **87**, 6803–6807 (1990).

11. M. L. Paddock *et al*., Pathway of proton transfer in bacterial reaction centers: Role of aspartate-L213 in proton transfers associated with reduction of quinone to dihydroquinone. *Biochemistry* **33**, 734–745 (1994).
12. H. L. Axelrod, E. C. Abresch, M. L. Paddock, M. Y. Okamura, G. Feher, Determination of the binding sites of the proton transfer inhibitors Cd^{2+} and Zn^{2+} in bacterial reaction centers. *Proc. Natl. Acad. Sci. U.S.A.* **97**, 1542–1547 (2000).
13. P. Maróti, D. K. Hanson, L. Baciou, M. Schiffer, P. Sebban, Proton conduction within the reaction centers of *Rhodobacter capsulatus*: The electrostatic role of the protein. *Proc. Natl. Acad. Sci. U.S.A.* **91**, 5617–5621 (1994).
14. L. Gerencsér, P. Maróti, Retardation of proton transfer caused by binding of the transition metal ion to the bacterial reaction center is due to pK_a shifts of key protonatable residues. *Biochemistry* **40**, 1850–1860 (2001).
15. L. Gerencser, A. Taly, L. Baciou, P. Maroti, P. Sebban, Effect of binding of Cd^{2+} on bacterial reaction center mutants: Proton-transfer uses interdependent pathways. *Biochemistry* **41**, 9132–9138 (2002).
16. H. Kuroda *et al*., Proton transfer pathway from the oxygen-evolving complex in photosystem II substantiated by extensive mutagenesis. *Biochim. Biophys. Acta Bioenerg.* **1862**, 148329 (2021).
17. P. Maróti, C. W. Wraight, Flash-induced H^+ binding by bacterial photosynthetic reaction centers: Influences of the redox states of the acceptor quinones and primary donor. *Biochim. Biophys. Acta* **934**, 329–347 (1988).
18. P. H. McPherson, V. Nagarajan, W. W. Parson, M. Y. Okamura, G. Feher, pH-dependence of the free energy gap between DQ_A and $D^+Q^-_A$ determined from delayed fluorescence in reaction centers from *Rhodobacter sphaeroides* R-26. *Biochim. Biophys. Acta* **1019**, 91–94 (1990).
19. R. Hienerwadel *et al*., Protonation of Glu L212 following Q_B^- formation in the photosynthetic reaction center of *Rhodobacter sphaeroides*: Evidence from time-resolved infrared spectroscopy. *Biochemistry* **34**, 2832–2843 (1995).
20. E. Nabedryk *et al*., Fourier transforms infrared difference spectroscopy of secondary quinone acceptor photoreduction in proton transfer mutants of *Rhodobacter sphaeroides*. *Biochemistry* **34**, 14722–14732 (1995).
21. J. Miksovska *et al*., Distant electrostatic interactions modulate the free energy level of Q_A^- in the photosynthetic reaction center. *Biochemistry* **35**, 15411–15417 (1996).
22. H. Ishikita, G. Morra, E.-W. Knapp, Redox potential of quinones in photosynthetic reaction centers from *Rhodobacter sphaeroides*: Dependence on protonation of Glu-L212 and Asp-L213. *Biochemistry* **42**, 3882–3892 (2003).
23. M. H. B. Stowell *et al*., Light-induced structural changes in photosynthetic reaction center: Implications for mechanism of electron-proton transfer. *Science* **276**, 812–816 (1997).
24. H. Ishikita, K. Saito, Proton transfer reactions and hydrogen-bond networks in protein environments. *J. R. Soc. Interface* **11**, 20130518 (2013).
25. C. A. Wraight, Proton and electron transfer in the acceptor quinone complex of photosynthetic reaction centers from *Rhodobacter sphaeroides*. *Front. Biosci.* **9**, 309–337 (2004).
26. K. Saito, M. Mandal, H. Ishikita, Redox potentials along the redox-active low-barrier H-bonds in electron transfer pathways. *Phys. Chem. Chem. Phys.* **22**, 25467–25473 (2020).
27. M. Kimura, Y. Kato, T. Noguchi, Protonation state of a key histidine ligand in the iron–quinone complex of photosystem II as revealed by light-induced ATR-FTIR spectroscopy. *Biochemistry* **59**, 4336–4343 (2020).
28. A. Warshel, A. Papazyan, P. A. Kollman, On low-barrier hydrogen bonds and enzyme catalysis. *Science* **269**, 102–106 (1995).
29. C. N. Schutz, A. Warshel, The low barrier hydrogen bond (LBHB) proposal revisited: The case of the Asp... His pair in serine proteases. *Proteins* **55**, 711–723 (2004).
30. C. L. Perrin, J. B. Nielson, "Strong" hydrogen bonds in chemistry and biology. *Annu. Rev. Phys. Chem.* **48**, 511–544 (1997).
31. Z. Zhu, M. R. Gunner, Energetics of quinone-dependent electron and proton transfers in *Rhodobacter sphaeroides* photosynthetic reaction centers. *Biochemistry* **44**, 82–96 (2005).
32. M. L. Paddock *et al*., ENDOR spectroscopy reveals light induced movement of the H-bond from Ser-L223 upon forming the semiquinone ($Q_B^{-\bullet}$) in reaction centers from *Rhodobacter sphaeroides*. *Biochemistry* **46**, 8234–8243 (2007).
33. M. L. Paddock, G. Feher, M. Y. Okamura, Identification of the proton pathway in bacterial reaction centers: Replacement of Asp-M17 and Asp-L210 with Asn reduces the proton transfer rate in the presence of Cd^{2+}. *Proc. Natl. Acad. Sci. U.S.A.* **97**, 1548–1553 (2000).
34. A. W. Roszak *et al*., New insights into the structure of the reaction centre from *Blastochloris viridis*: Evolution in the laboratory. *Biochem. J.* **442**, 27–37 (2012).
35. H. L. Axelrod *et al*., X-ray structure determination of the cytochrome c_2: Reaction center electron transfer complex from *Rhodobacter sphaeroides*. *J. Mol. Biol.* **319**, 501–515 (2002).
36. A. K. Grafton, R. A. Wheeler, Amino acid protonation states determine binding sites of the secondary ubiquinone and its anion in the *Rhodobacter sphaeroides* photosynthetic reaction center. *J. Phys. Chem. B* **103**, 5380–5387 (1999).
37. B. Rabenstein, G. M. Ullmann, E.-W. Knapp, Electron transfer between the quinones in the photosynthetic reaction center and its coupling to conformational changes. *Biochemistry* **39**, 10487–10496 (2000).
38. H. Ishikita, E.-W. Knapp, Energetics of proton transfer pathways in reaction centers from *Rhodobacter sphaeroides*. The Glu-H173 activated mutants. *J. Biol. Chem.* **280**, 12446–12450 (2005).
39. H. Ishikita, E.-W. Knapp, Control of quinone redox potentials in photosystem II: Electron transfer and photoprotection. *J. Am. Chem. Soc.* **127**, 14714–14720 (2005).
40. M. L. Paddock *et al*., Identification of the proton pathway in bacterial reaction centers: Cooperation between Asp-M17 and Asp-L210 facilitates proton transfer to the secondary quinone (Q_B). *Biochemistry* **40**, 6893–6902 (2001).
41. M. L. Paddock, M. S. Graige, G. Feher, M. Y. Okamura, Identification of the proton pathway in bacterial reaction centers: Inhibition of proton transfer by binding of Zn^{2+} or Cd^{2+}. *Proc. Natl. Acad. Sci. U.S.A.* **96**, 6183–6188 (1999).
42. P. Ädelroth *et al*., Identification of the proton pathway in bacterial reaction centers: Decrease of proton transfer rate by mutation of surface histidines at H126 and H128 and chemical rescue by imidazole identifies the initial proton donors. *Biochemistry* **40**, 14538–14546 (2001).
43. M. L. Paddock, G. Feher, M. Y. Okamura, Proton transfer pathways and mechanism in bacterial reaction centers. *FEBS Lett.* **555**, 45–50 (2003).
44. S. Niwa *et al*., Structure of the LH1-RC complex from *Thermochromatium tepidum* at 3.0 Å. *Nature* **508**, 228–232 (2014).
45. D. A. Cherepanov *et al*., Reduction and protonation of the secondary quinone acceptor of *Rhodobacter sphaeroides* photosynthetic reaction center: Kinetic model based on a comparison of wild-type chromatophores with mutants carrying Arg→Ile substitution at sites 207 and 217 in the L-subunit. *Biochim. Biophys. Acta* **1459**, 10–34 (2000).
46. S. Osváth, P. Maróti, Coupling of cytochrome and quinone turnovers in the photocycle of reaction centers from the photosynthetic bacterium *Rhodobacter sphaeroides*. *Biophys. J.* **73**, 972–982 (1997).
47. N. Sakashita, H. C. Watanabe, T. Ikeda, K. Saito, H. Ishikita, Origins of water molecules in the photosystem II crystal structure. *Biochemistry* **56**, 3049–3057 (2017).
48. E. C. Abresch *et al*., Identification of proton transfer pathways in the X-ray crystal structure of the bacterial reaction center from *Rhodobacter sphaeroides*. *Photosynth. Res.* **55**, 119–125 (1998).
49. B. R. Brooks *et al*., CHARMM: A program for macromolecular energy, minimization, and dynamics calculations. *J. Comput. Chem.* **4**, 187–217 (1983).
50. A. D. MacKerell Jr *et al*., All-atom empirical potential for molecular modeling and dynamics studies of proteins. *J. Phys. Chem. B* **102**, 3586–3616 (1998).
51. K. Kawashima, H. Ishikita, Energetic insights into two electron transfer pathways in light-driven energy-converting enzymes. *Chem. Sci. (Camb.)* **9**, 4083–4092 (2018).
52. D. Bashford, M. Karplus, pK_a's of ionizable groups in proteins: Atomic detail from a continuum electrostatic model. *Biochemistry* **29**, 10219–10225 (1990).
53. Y. Nozaki, C. Tanford, Acid-base titrations in concentrated guanidine hydrochloride. Dissociation constants of the guamidinium ion and of some amino acids. *J. Am. Chem. Soc.* **89**, 736–742 (1967).
54. M. Tanokura, ^{1}H nuclear magnetic resonance titration curves and microenvironments of aromatic residues in bovine pancreatic ribonuclease A. *J. Biochem.* **94**, 51–62 (1983).
55. M. Tanokura, ^{1}H-NMR study on the tautomerism of the imidazole ring of histidine residues. I. Microscopic p*K* values and molar ratios of tautomers in histidine-containing peptides. *Biochim. Biophys. Acta* **742**, 576–585 (1983).
56. M. Tanokura, ^{1}H-NMR study on the tautomerism of the imidazole ring of histidine residues. II. Microenvironments of histidine-12 and histidine-119 of bovine pancreatic ribonuclease A. *Biochim. Biophys. Acta* **742**, 586–596 (1983).
57. B. Rabenstein, E.-W. Knapp, Calculated pH-dependent population and protonation of carbon-monoxy-myoglobin conformers. *Biophys. J.* **80**, 1141–1150 (2001).
58. QSite, Version 5.8 (Schrödinger, New York, NY, 2012).
59. G. Vacek, J. K. Perry, J. M. Langlois, Advanced initial-guess algorithm for self-consistent-field calculations on organometallic systems. *Chem. Phys. Lett.* **310**, 189–194 (1999).
60. D. Beglov, B. Roux, An integral equation to describe the solvation of polar molecules in liquid water. *J. Phys. Chem. B* **101**, 7821–7826 (1997).
61. A. Kovalenko, F. Hirata, Potential of mean force between two molecular ions in a polar molecular solvent: A study by the three-dimensional reference interaction site model. *J. Phys. Chem. B* **103**, 7942–7957 (1999).
62. T. Luchko *et al*., Three-dimensional molecular theory of solvation coupled with molecular dynamics in Amber. *J. Chem. Theory Comput.* **6**, 607–624 (2010).
63. D. A. Case *et al*., *AMBER 12* (University of California, San Francisco, 2012).
64. D. J. Sindhikara, N. Yoshida, F. Hirata, Placevent: An algorithm for prediction of explicit solvent atom distribution-application to HIV-1 protease and F-ATP synthase. *J. Comput. Chem.* **33**, 1536–1543 (2012).
65. T. Takaoka, N. Sakashita, K. Saito, H. Ishikita, pK_a of a proton-conducting water chain in photosystem II. *J. Phys. Chem. Lett.* **7**, 1925–1932 (2016).
66. X. Wei *et al*., Structure of spinach photosystem II-LHCII supercomplex at 3.2 Å resolution. *Nature* **534**, 69–74 (2016).
67. J. Breton, Absence of large-scale displacement of quinone Q_B in bacterial photosynthetic reaction centers. *Biochemistry* **43**, 3318–3326 (2004).